Large-eddy simulation of a boundary layer with concave streamwise curvature

By T. S. Lund

1. Motivation and objectives

Turbulence modeling continues to be one of the most difficult problems in fluid mechanics. Existing prediction methods are well developed for certain classes of simple equilibrium flows, but are still not entirely satisfactory for a large category of complex non-equilibrium flows found in engineering practice. Direct and large-eddy simulation (LES) approaches have long been believed to have great potential for the accurate prediction of difficult turbulent flows, but the associated computational cost has been prohibitive for practical problems. This remains true for direct simulation but is no longer clear for large-eddy simulation. Advances in computer hardware, numerical methods, and subgrid-scale modeling have made it possible to conduct LES for flows of practical interest at Reynolds numbers in the range of laboratory experiments. A handful of these simulations have been performed over the last few years (*cf.* Akselvoll and Moin 1993, Zang *et al.* 1993, He and Song, 1993). Many of these recent simulations were performed to develop LES technology for complex flows and assess the accuracy of the dynamic subgrid-scale model. The indication from these first simulations is that LES in conjunction with the dynamic model is capable of accurately predicting high Reynolds number complex flows for which Reynolds-averaged techniques have not been able to produce satisfactory results. The validation and technology development phase for LES of complex flows is ongoing, and additional challenging test cases must be attempted. The objective of this work is to apply LES and the dynamic subgrid-scale model to the flow of a boundary layer over a concave surface.

Although the geometry of a concave wall is not very complex, the boundary layer that develops on its surface is difficult to model due to the presence of streamwise Taylor-Görtler vortices. These vortices arise as a result of a centrifugal instability associated with the concave curvature. The vortices are of the same scale as the boundary layer thickness, alternate in sense of rotation, and are strong enough to induce significant changes in the boundary layer statistics. Owing to their streamwise orientation and alternate signs, the Taylor-Görtler vortices induce alternating bands of flow toward and away from the wall. The induced upwash and downwash motions serve as effective agents to transport streamwise momentum normal to the wall, thereby increasing the skin friction. Reynolds-averaged prediction techniques are unable to resolve these vortices and must resort to *ad hoc* correction terms. Aside from Taylor-Görtler vortices, concave curvature affects the turbulent Reynolds stress budget. This effect is captured in full Reynolds stress models but is absent in the more commonly used algebraic, one- or two-equation models.

In contrast to Reynolds-averaged approaches, LES is well suited for the concave-wall boundary layer flow since the Taylor-Görtler vortices are simulated directly. In addition, the effects of curvature, not associated with vortices, are captured.

The simulations reported here are designed to match the laboratory experiments of Barlow and Johnston (1988) and Johnson and Johnston (1989). These experiments are an ideal test case since a rather complete set of velocity statistics are available for several streamwise stations.

2. Accomplishments

2.1 Numerical method

The computer code used for this project is based on the second-order staggered mesh finite difference algorithm described by Choi and Moin (1994). The incompressible Navier-Stokes equations are integrated in time with a fully implicit variant of the fractional step algorithm. Generalized curvilinear coordinates are used in two directions with the third direction (usually spanwise) restricted to be uniform. In the fractional step procedure, the dependent variables are advanced in a two-step process where an intermediate velocity field is first advanced without the pressure gradient term. The effect of the pressure gradient is then accounted for through a correction term obtained by solving a Poisson equation. In the current implementation, the intermediate velocity field is advanced with a fully-implicit scheme where Newton iteration is used to reduce the factorization error. By taking a Fourier transform in uniform mesh direction (spanwise), the Poisson equation is reduced to a series of two dimensional problems, one for each spanwise wavenumber. The lowest wavenumber system is solved with a direct inversion technique, whereas the higher wavenumber systems are treated with a Gauss-Seidel iteration scheme. Although the scheme is stable for CFL numbers of at least 5, the time step is usually dictated by accuracy requirements. In this work, the maximum CFL number is held below 2.0.

2.2 Computational domain and flow conditions

The simulations are designed to match the laboratory configuration of Barlow and Johnston (1988) and Johnson and Johnston (1989). The experimental facility is a water channel where a straight entry flow section is fitted to a 90° constant radius of curvature bend (see Fig. 1). The opposite wall is contoured in order to minimize the streamwise pressure gradient on the concave wall. Boundary layers develop on both channel walls; one experiences an abrupt transition to concave curvature while the other experiences a transition to convex curvature. Measurements are available only for the concave side. Both boundary layers are tripped early on the entry section and become fully turbulent by the beginning of the curved section. At this station, the two boundary layers are separated by about 1.5 boundary layer thicknesses of potential core in the center of the channel. The potential core diminishes with downstream distance, and the two boundary layers merge between the 75° and 90° stations. The momentum thickness Reynolds number at the beginning of the curve is $R_{\theta_0} = 1300$. At this station, the ratio of boundary layer thickness to radius of

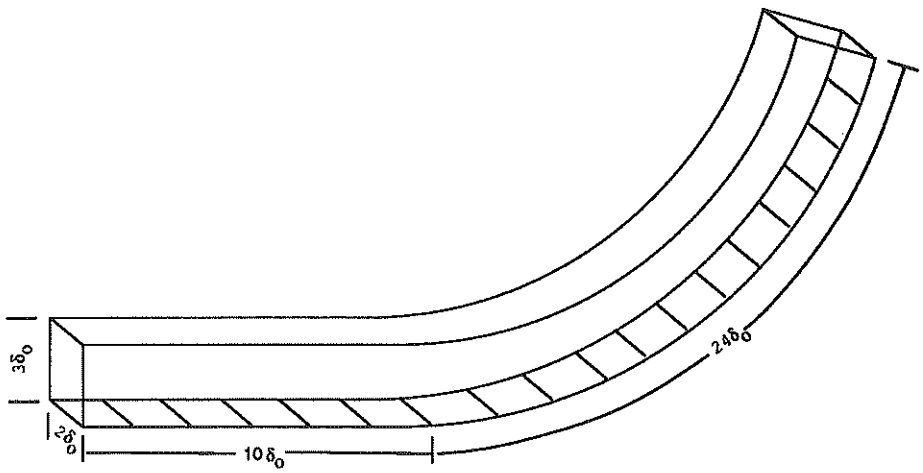

FIGURE 1. Computational domain. All dimensions are referred to the boundary layer thickness measured at the location where the curvature begins (δ_0). The radius of curvature is $R = 18.1\delta_0$.

curvature, δ_0/R, is 0.055, which is sufficiently large to create significant curvature effects.

The computational domain is an abbreviated version of the experimental geometry. A sketch is provided in Fig. 1. The calculation begins approximately 10 boundary layer thicknesses upstream of the curved section and ends at the 75° station (the boundary layer thickness measured at the onset of curvature, δ_0 is used as the normalizing length scale). Unsteady turbulent boundary layer data are supplied at the inflow boundary whereas a convective boundary condition is used at the outflow boundary. The domain extends $2\delta_0$ in the spanwise direction and periodic boundary conditions are used in this direction. According to the experimental measurements, the spanwise width is sufficient to enclose 4 streamwise Taylor-Görtler vortices. Only the concave boundary layer is simulated, and consequently the domain extends from the concave wall to the streamline that lies along the channel centerline. No slip conditions are applied at the solid wall whereas impermeable and no-stress conditions are applied at the upper boundary. The position of the streamline boundary is determined by conducting an inviscid analysis of the experimental geometry. The displacement effects of both boundary layers is accounted for in this analysis.

The computational grid contains $358 \times 44 \times 64$ points in the streamwise, wall-normal, and spanwise directions respectively. The mesh is stretched in the wall-normal direction and uniform in the other two. The grid spacings, based on wall units at the location where the curve begins, are $\Delta x^+ = 50$, $\Delta y^+_{\min} = 1$, and

$\Delta z^+ = 16$.

2.3 Inflow boundary data

A spatially-evolving simulation such as this one requires the specification of instantaneous turbulent data at the inflow boundary. Accurate inflow data is required to insure that the boundary layer is fully turbulent and in equilibrium at the beginning of the curve. Instantaneous inflow data is generated via an auxiliary large-eddy simulation of a flat plate boundary layer. This simulation is also spatially evolving, but makes use of Spalart's method (1988) to generate its own inflow data by rescaling the data at the exit station. The resolution of the inflow simulation is identical to that of the main simulation. The inflow simulation is run in parallel with the main simulation in a time-synchronous fashion. At each time step, the velocity field is extracted from an appropriate $y - z$ plane in the inflow simulation. This data is used directly as the inflow boundary conditions. In practice, the inflow simulation can be either run at the same time as the main simulation or run ahead of time and the inflow data stored on disk. The inflow simulation increases the overall cost of the main simulation by about 10%.

2.4 Simulation results

Before sampling statistics, the simulation is run for an initial transient elimination period of 45 boundary layer inertial time scale units (1.2 flow-through times). Statistics are then sampled over a period of 150 inertial time scales (3.9 flow-through times). Mean quantities are formed by averaging over both the spanwise direction and time.

The pressure distribution on the concave wall is compared with the experimental measurements in Fig. 2. The curve begins at $x = 0$, and thus negative values of x correspond to the flat entry section. Overall, the pressure is reasonably constant. The largest pressure gradient occurs near the start of the curve. This is due to slight errors in the contour applied to the upper streamline. Since the streamline was determined through an inviscid analysis of the experimental configuration, it is quite likely that a similar pressure signature exists in the experiment. Unfortunately no detailed measurements are available in the region near the start of the curve. The maximum deviation from uniform pressure is roughly 2%, which probably has a negligible effect on the boundary layer development. Aside from the pressure variation near the start of the curve, there is a small uniform drop in pressure with streamwise distance. This is due to a slight acceleration of the core flow resulting from errors made in the estimate for the boundary layer displacement thickness used to determine the upper streamline. The enhanced pressure drop near the downstream boundary is due to inaccuracies in the outflow boundary condition.

Mean velocity profiles at several streamwise stations are compared with the experimental data in Fig. 3. The first station is on the flat inlet section, 8 boundary layer thicknesses ahead of the curved section. The next 4 stations are at 15°, 30°, 45°, and 60° (4.7, 9.5, 14.2, and 18.9 boundary layer thicknesses into the curved section). The velocity data are normalized with the velocity profile that would be developed by an inviscid flow through the curved section. To a good approximation,

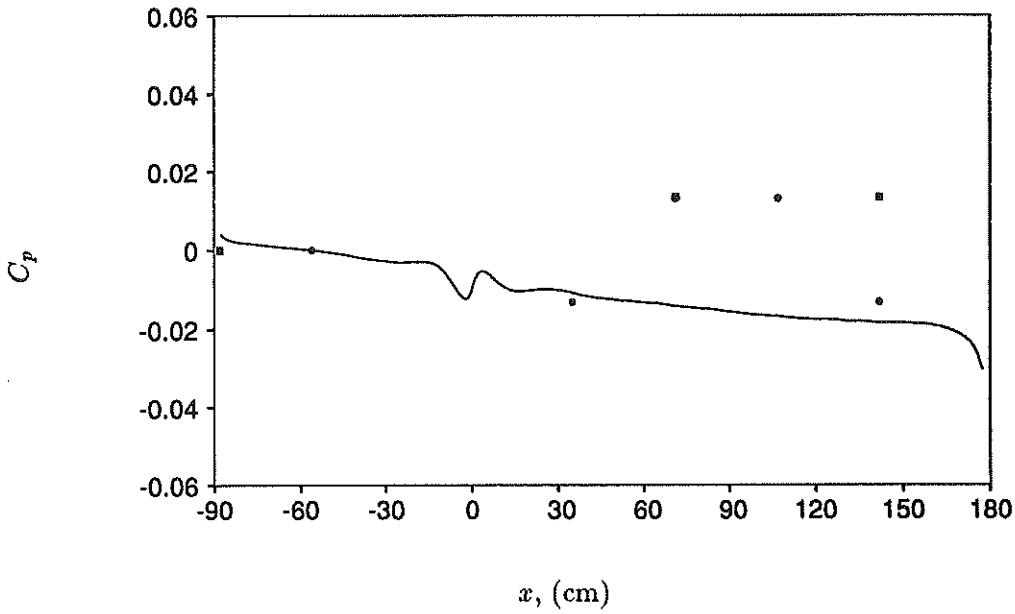

FIGURE 2. Pressure distribution on the concave wall. The curve begins at $x = 0$. δ_0 is the boundary layer thickness at $x = 0$. ——— : LES; ● : Johnson and Johnston (1989); ■ : Barlow and Johnston (1988). In the experiments, the pressure is determined indirectly from the velocity measured in the potential core region.

this profile varies linearly according to

$$U_p(y) \simeq U_{pw}(1 + y/R), \tag{1}$$

where U_{pw} is the inviscid velocity that would be achieved at the wall. Overall, the agreement between simulation and experiment is quite good. On the flat section, the simulation produces profiles that are a bit fuller near the wall as compared with the experiment. This discrepancy is related to the grid resolution and can be reduced by refining the streamwise and spanwise mesh spacings. The current level of agreement is deemed acceptable, however. The initial discrepancy fades in the curved section. Note the difference in the shape of the profile between the flat and 60° stations (first and last curves in Fig. 3). The effect of concave curvature is to create fuller profiles, especially close to the wall. This is due to enhanced mixing resulting from the effects of curvature.

Reynolds shear stress profiles are shown in as the solid lines in Fig. 4 (the dashed lines will be described below). Overall, the agreement with the experimental data is reasonable. The simulation does a good job of capturing the qualitative changes to the shear stress profile that result from concave curvature. The peak Reynolds stress increases and the profile develops a bulge in the central region of the profile. On a quantitative level, however, the simulation tends to under-predict the peak Reynolds stress, especially at the 45° and 60° stations. The reason for this discrepancy is not

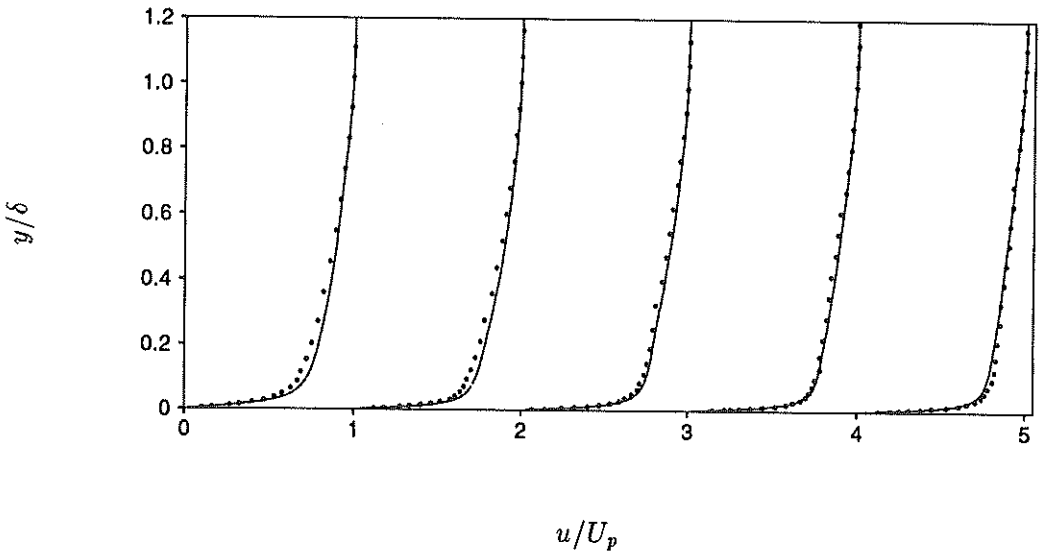

FIGURE 3. Mean streamwise velocity profiles. The velocity is scaled by $U_p(y)$ (Eq. (1)), the streamwise profile that would be developed in an inviscid flow through the curved section. The first station is on the flat inlet section, 8 boundary layer thicknesses ahead of the curve. The next 4 stations are at 15°, 30°, 45°, and 60° respectively. ——— : LES; • : Johnson and Johnston (1989).

fully understood, but there is some evidence that it is related to the details of the inflow conditions. An example of the sensitivity to inflow conditions is shown by the dashed lines in Fig. 4, where an alternative set of inflow data is used. In this case, inflow is generated from a parallel-flow boundary layer simulation. The instantaneous velocity data from this simulation is rescaled to yield statistics that are consistent with a spatially-evolving boundary layer. The rescaling operation is not sufficiently accurate to keep the boundary layer in equilibrium, and a transient develops near the inflow boundary. This effect is clearly visible in Fig. 4 where the Reynolds stress is over-predicted at the first measurement station. Although it may be fortuitous, higher levels of Reynolds stress on the flat section lead to considerably better agreement with the experimental data at the downstream stations. Future work will focus on a through understanding of this effect.

Velocity fluctuations are compared with the experiment in Fig. 5. Agreement with the experimental data is good. Again the qualitative changes to the profiles resulting from concave curvature are well reproduced. A bulge develops in the central portion of each profile. This effect is greatest for the wall-normal and spanwise fluctuations. On a quantitative level, minor differences exist between the simulation and experiment. Except for the near-wall region of the streamwise profile, all three velocity fluctuations are generally under-predicted in the simulation. The

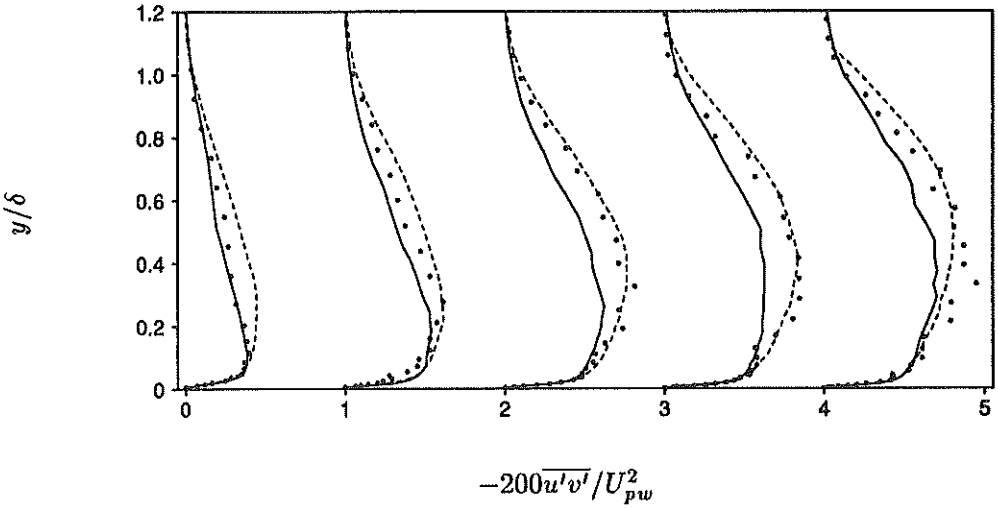

FIGURE 4. Reynolds shear stress profiles. ——— : LES, spatially evolving boundary layer inflow data; ---- : LES, rescaled parallel flow boundary layer inflow data; • : experimental measurements of Johnson and Johnston (1989). The first station is on the flat inlet section, 8 boundary layer thicknesses ahead of the curve. The next 4 stations are at 15°, 30°, 45°, and 60° respectively. U_{pw} is an extrapolation of the core velocity to the wall assuming an inviscid profile.

reason for this discrepancy is not completely understood, but as in the case of the Reynolds shear stress, it is sensitive to the inflow conditions. Better agreement can be obtained at the downstream stations if the fluctuation levels are increased at the inlet. Aside from these differences, the velocity fluctuations are too anisotropic near the wall; the streamwise fluctuation is over-predicted whereas the wall-normal and especially spanwise fluctuations are under-predicted. This is a common symptom of marginal resolution in either a direct or large-eddy simulation. It is caused by an inability to resolve the inter-component energy transfer mechanism in this region of the flow. The discrepancy can be reduced by increasing the number of grid points, but current level of agreement is deemed acceptable.

The calculated skin friction is compared with experiment in Fig. 6. The skin friction is seen to increase significantly due to the effects of concave curvature. The simulation captures this trend but also exhibits some quantitative differences with the experimental data. The simulation results agree best with the experiment on the flat section ahead of the curve and beyond about 45° in the curved section. In the intermediate section, the simulated skin friction appears to respond more rapidly than the experiment downstream of the start of the curved section. The small excursion immediately upstream of the curved section is due to the residual pressure gradient in this region (see Fig. 2). Skin friction was determined in the experiment by fitting a log-law to the velocity profiles (Clauser chart approach). This method is accurate for equilibrium boundary layers but can be in significant

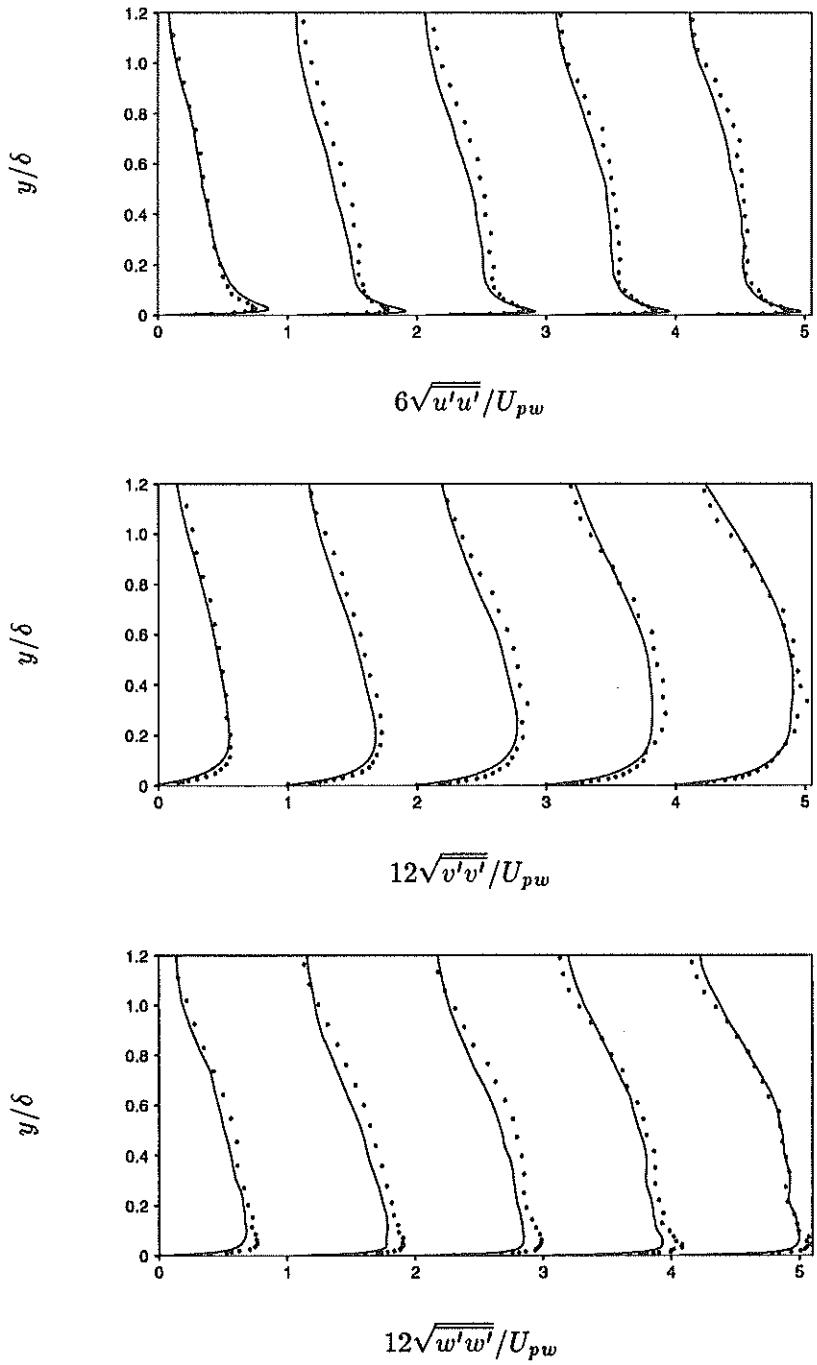

FIGURE 5. Velocity fluctuation profiles. The first station is on the flat inlet section, 8 boundary layer thicknesses ahead of the curve. The next 4 stations are at 15°, 30°, 45°, and 60° respectively. U_{pw} is an extrapolation of the core velocity to the wall assuming an inviscid profile. ——— : LES; • : experimental measurements of Johnson and Johnston (1989).

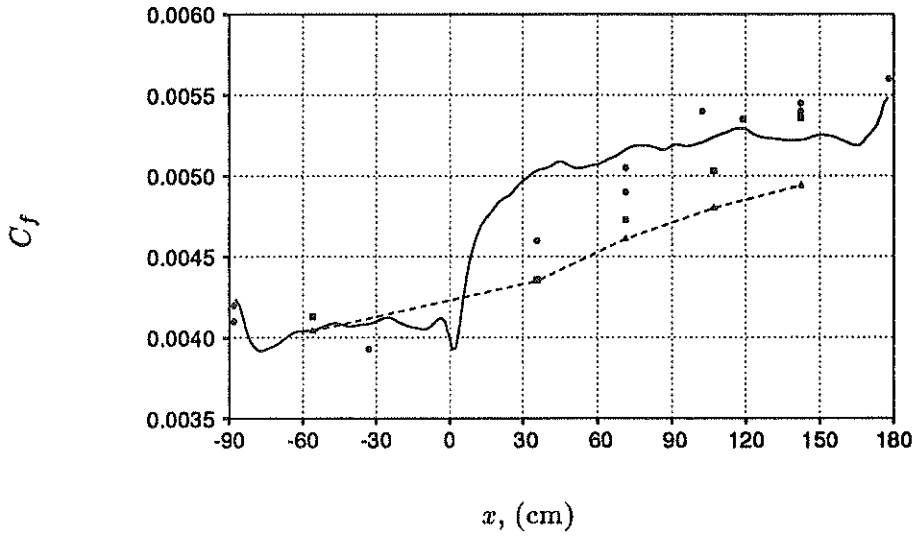

FIGURE 6. Skin friction coefficient. The curve begins at $x = 0$. ——— : LES, direct method; ● : experimental data of Johnson and Johnston; ■ : experimental data of Barlow and Johnston; --▲-- : LES, Clauser method.

error when applied in non-equilibrium situations. Since the boundary layer is displaced from equilibrium while transitioning from the flat to curved sections, the experimental skin friction measurements could be in error. In order to assess this possibility, skin friction was determined from the simulation data indirectly through use of the Clauser chart. The results of these measurements are shown as the triangles connected with a dashed line in Fig. 6. As expected, there are significant differences between the direct measurement and the Clauser method near the onset of curvature. In particular, the Clauser method measurements fall below the direct measurements near the onset of curvature and are actually in better agreement with the experimental data in this region. As the boundary layer comes into equilibrium further downstream, the Clauser and direct measurements appear to be converging.

2.5 Conclusions

Large-eddy simulations of a concave-wall boundary layer have been performed. The simulations make use of the dynamic subgrid-scale model which requires neither the tuning of model constants, nor the use of *ad hoc* corrections for curvature. Concave curvature results in large changes to the turbulent statistics, and LES does a good job of predicting the transition from a flat wall to a concave surface. Quantitative differences exist between the LES results and the experimental data, and these can be attributed in part to the details of the turbulent data supplied at the inflow boundary. The turbulent flow fields do not reveal strong Taylor-Görtler vortices, a feature that may also be related to the inflow data. In the experiment, streamwise vorticity is generated by the flow-conditioning devices and is amplified in the contraction leading to the channel. These vortices may act as effective nuclei

for the rapid development of Taylor-Görtler vortices in the curved section. In the simulations, coherent streamwise vorticity is absent from the outer regions of the spatially-evolving boundary layer inflow data. Stream-wise vortices are probably also absent in the outer portion of the parallel flow boundary layer data, although the rescaling operation results in higher fluctuations in this region of the profile. In any case, Taylor-Görtler vortices will develop eventually from the background turbulence, but the organization process may require a streamwise distance that is a function of the initial velocity fluctuation level. In order to avoid this uncertainty, it may be necessary to "seed" the outer regions of the inflow boundary layer with semi-coherent streamwise vorticity corresponding to the levels existing in the experiment.

3. Future plans

Future work will focus on a careful study of the influence of inflow conditions. In particular, streamwise vorticity will be introduced to the outer region of the inflow boundary layer. The flow fields will be examined for the presence of strong Taylor-Görtler vortices and the results compared with the existing runs. Once issues with the inflow data are resolved, the impact of the subgrid-scale model will be investigated. This will be done by repeating the simulation with no subgrid-scale model. Differences between the runs with and without the model will help elucidate the influence of the subgrid-scale model in this flow.

The LES results will also be compared with the predictions of Reynolds averaged Navier-Stokes (RANS) calculations. Aside from full Reynolds stress closure, RANS methods have no formal dependence on curvature. *Ad hoc* corrections are commonly used to account for curvature and the accuracy of a few of these will be investigated. Full Reynolds stress models do have a curvature-dependent production term, and the effect of this term will be investigated.

REFERENCES

AKSELVOLL, K. & MOIN, P. 1993 Application of the dynamic localization model to large-eddy simulation of turbulent flow over a backward-facing step. In *Engineering applications of large-eddy simulations*, ed. by S. A. Ragab and U. Piomelli. Presented at the ASME fluid engineering conference, Washington D. C. June 20-24, 1993.

BARLOW, R. S. & JOHNSTON, J. P. 1988 Structure of a turbulent boundary layer on a concave surface. *J. Fluid Mech.* **191**, 137-176.

CHOI, H., MOIN, P. & KIM J. 1993 Direct numerical simulation of turbulent flow over riblets. *J. Fluid Mech.* **255**, 503-540.

HE, J., & SONG, C. C. S., 1993 Some applications of large-eddy simulation to large-scale turbulent flows at small Mach number. In *Engineering applications of large-eddy simulations*, ed. by S. A. Ragab and U. Piomelli. Presented at the ASME fluid engineering conference, Washington D. C. June 20-24, 1993.

JOHNSON, P. L., & JOHNSTON, J. P. 1989 The effects of grid-generated turbulence on a flat and concave turbulent boundary layer, Report MD-53, Thermosciences Division, Dept. of Mech. Eng., Stanford University.

SPALART, P. R. 1988 Direct simulation of a turbulent boundary layer up to $R_\theta =$ 1410. *J. Fluid Mech.* **187**, 61-98.

ZANG, Y., STREET, R. L., & KOSEFF, J. R. 1993 A dynamic mixed subgrid-scale model and its application to recirculating flows. *Phys. Fluids A.* **5**, 3186-3196.